2025 IEEE 36th International Symposium on Personal, Indoor and Mobile Radio Communications (PIMRC) | 979-8-3503-6323-4/25/$31.00 ©2025 IEEE | DOI: 10.1109/PIMRC62392.2025.11275523

Sensing Topology Management in 6G Integrated Sensing and Communications Systems

Giacomo Mazzola
Delft University of Technology
Delft, The Netherlands
gmazzola99@gmail.com

Sakshi Agarwal
TNO
The Hague, The Netherlands
sakshi.agarwal@tno.nl

Kallol Das
TNO
The Hague, The Netherlands
kallol.das@tno.nl

Remco Litjens
TNO
The Hague, The Netherlands
Delft University of Technology
Delft, The Netherlands
remco.litjens@tno.nl

Haibin Zhang
TNO
The Hague, The Netherlands
haibin.zhang@tno.nl

***Abstract*—We develop and assess radio resource management solutions for Integrated Sensing and Communications (ISAC) in 6G networks. A novel sensing topology management scheme is introduced to balance trade-offs between sensing/communication performance and resource consumption. The simulation results demonstrate the impact of the configuration of the sensing topology management scheme on the selected and the effective topology sizes, while further quantifying the sensitivity of the sensing/communication performance w.r.t. the topology size, the number of present active- and idle-mode UEs, the number of sensing tasks, the network deployment density and the radar cross section of sensing targets. This study provides valuable insights for the effective deployment and management of sensing services in 6G mobile networks.**

Keywords—6G, ISAC, radio resource management, sensing topology management, probability of detection, user throughput performance, system-level simulations

I. Introduction

Integrated Sensing and Communication (ISAC) technology, a cornerstone of the emerging sixth generation of mobile communication (6G), seeks to harness new business potentials by merging sensing and communication services into a single unified system [1]. This integration can range from basic infrastructure and spectrum sharing to advanced waveform/signal sharing between sensing and communication functions. While tight integration is envisioned to optimise resource efficiency, the exploitation of this potential imposes important challenges in waveform design, resource management and network deployment, incl. the design of coordinated solutions in sensing-aided communications and communications-aided sensing. Unlike communication tasks, sensing tasks often rely on the involvement of multiple transmitters and receivers, imposing a challenge in topology management, including node selection and the assignment of transmitter and receiver roles within a dynamic cellular network.

Most works on radio resource management in ISAC systems focus on single-cell scenarios, addressing link- or system-level optimisation. [2] introduces a power allocation and spectrum partitioning algorithm to optimise Quality of Service (QoS) and energy consumption in an ISAC system. Similarly, [3] explores resource scheduling in Orthogonal Time Frequency Space-based ISAC systems, enhancing the sum rate for multiple users while adhering to power and Cramer-Rao Bound constraints to improve sensing and communication performance. Considering multi-cell ISAC, [4] proposes a framework to optimise cell-user association to minimise inter-cell interference and control transmission power in order to balance signal quality and energy consumption. [5] presents a unified resource allocation framework for power and bandwidth sharing, balancing QoS over detection, tracking and surveillance applications, while optimising sensing and communication performance. [6] considers the conceptual notion of topology management and switching based on observed sensing performance, however no concrete topology selection algorithms are proposed/analysed. In [7] all (and only) base stations (BSs) are assumed to be involved in a given sensing task, with the proposed algorithm merely in charge of assigning their role as either transmitter or receiver. Lastly, [8] considers selecting nodes to be involved in a sensing task, applying mono-static sensing and decision-level fusion after the per-node derivation of a detection/false alarm probability.

Despite these research endeavours, the ISAC literature still lacks low-complexity solutions for real-time integrated topology management and role assignment, able to deal with the dynamic nature of cellular networks and a diversity of available (BS or UE) nodes. To the best of our knowledge this work is the first to develop and assess solutions for sensing topology selection in dynamic multi-cell/user cellular networks jointly performing distributed sensing and communication tasks, considering both BSs and user devices (user equipments; UEs). We develop an advanced model for a communication-centric ISAC system that considers realistic propagation channels and interference between sensing and communication tasks. The proposed topology selection algorithm can be flexibly configured to balance the attained sensing performance (detection probability), the used resources and the communication performance. Motivated by the unpredictability of multipath fading dynamics, a distinction is made between the nodes selected for the transmission and reception of sensing signals (‘selected topology’), and the subset of those involved in the bottom-line sensing fusion (‘effective topology’).

979-8-3503-6323-4/25/$31.00 ©2025 IEEE

Furthermore, we extend an existing scheduling algorithm to support tempo-spatial multiplexing of sensing and communication tasks to further enhance resource efficiency.

The rest of the paper is organised as follows. Section II details the network, environment and service modelling aspects. Section III describes the radio resource management algorithms, incl. sensing topology management and resource scheduling. The system-level assessment approach is outlined in Section IV. Section V defines the evaluation scenarios and discusses the obtained results. Concluding remarks are given in Section VI.

II. Modelling

A. Network and device aspects

We consider a hexagonal network layout of sectorised sites deployed in a dense urban environment at a default inter-site distance (ISD) of *125* m, as visualised in Figure 1 . Each of the seven dark blue-shaded 'evaluation cells' is served by a BS equipped per cell with a 7^o-tilted 64T64R antenna array of cross-polarised antenna elements modelled as specified in [9]. Each cell is assigned an OFDM carrier with a $B = 20$ MHz bandwidth in the *7.1875* GHz band, configured with a *30* kHz subcarrier spacing, a TTI (Transmission Time Interval) duration of $T_{TTI} = 0.5$ ms and a total of $N_{PRBs} = 51$ PRBs (Physical Resource Blocks). Each BS is further characterised by a height of *10* m, a maximum cell transmit power of $p_{MAX} = 120$ W and a receiver noise figure of *2* dB. The performance assessment will focus on these evaluation cells, serving explicitly modelled sensing and communication tasks. The light blue-shaded 'background cells' serve no explicit traffic but are assumed to transmit at a fixed power of $0.5 \times p_{MAX}$ with a wide-area radiation pattern taken from [10], to establish realistic interference levels.

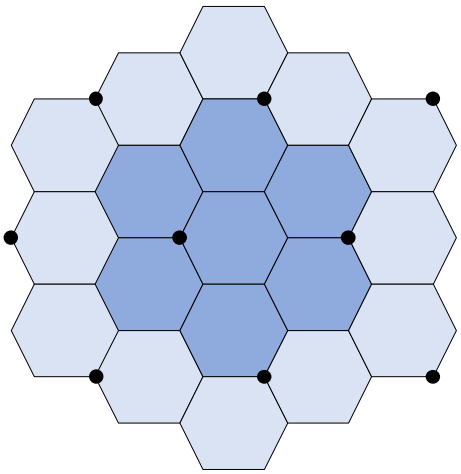

Figure 1: Network layout comprising evaluation (dark blue) and background (light blue) cells.

A configurable number N_{active} of active-mode UEs is randomly placed in each of the evaluation cells, applying a spatially uniform distribution. All active-mode UEs are engaged in a data communications flow. Additionally, a configurable number N_{idle} of idle-mode UEs is randomly placed in the area served by the evaluation cells. All UEs are at a fixed height of *1.5* m, equipped with a 1T4R antenna, comprising omni-directional antenna elements with a *0* dBi gain and are further characterised by a receiver noise figure of *8* dB. Both active- and idle-mode UEs may be selected into a sensing topology (see below) and contribute to the handling of sensing tasks.

B. Propagation environment

The path loss, shadowing and small-scale fading aspects are characterised based on the detailed UMi LoS mod**el** specified in [9] (implemented by [11]), while a comparsion with the NLoS model is made for a selected default scenario. The small-scale fading dynamics are caused by an assumed local mobility (at *0.8* m/s velocity) of the sensing targets and UEs. The channel response matrix of the link between nodes m and n is denoted by $\boldsymbol{H}_{m,n}(t,f)$ at TTI t and PRB f, where the nodes can represent a cell, UE or sensing target. The matrix dimensions reflect the number of antennas at the respective nodes, with the (isotropically radiating) sensing target modelled to comprise a single antenna. The average channel gain $G_{m,n}$ between nodes m and n is determined by the antenna gain, distance-based path loss and correlated shadowing, with an assumed *4* dB (*7.82* dB) standard deviation for the UMi LoS (NLoS) environment and a correlation coefficient of *0.5*.

C. Service characteristics

Sensing tasks entail the detection of target objects, with a configurable number $N_{sensing}$ of such targets randomly placed in the area served by the evaluation cells. The targets are modelled as spherical objects which radiate isotropically and whose size is characterised by an assumed default RCS (Radar Cross Section) [12] of $\sigma = 10$ m^2. Sensing tasks are performed by a topology of one or more transmitter/receiver nodes, with a sensing signal concurrently sent out by the transmitter nodes with an assumed periodicity of $T_{sensing} = 5$ TTIs. Key performance metric relevant to sensing is the probability of detection. *Communication* tasks are modelled as persistent full-buffer downlink data transfers to active-mode UEs, with the user-level throughput used as a key performance metric.

III. Radio Resource Management

This section outlines the distinct radio resource management algorithms, covering sensing topology management, cell selection, scheduling and beamforming.

A. Sensing topology management

Sensing topology management entails the selection of cell and/or UE nodes involved in conducting a given sensing task s, including an assignment of the transmitter/receiver roles. We herein assume that selected cells will take on both roles, while selected UEs can only act as receivers. In our solution, the sensing topology Ω is determined as

$$\Omega = \left\{ m \in \Xi \cup \Phi : G_{m,s} \geq G_{max} \cdot 10^{-\gamma/10} \right\} \cup \left\{ \underset{c \in \Xi}{\operatorname{argmax}}\, G_{c,s} \right\}$$

with

$$G_{max} = \max_{m \in \Xi \cup \Phi} G_{m,s},$$

and where Ξ comprises the evaluation cells and Φ includes all candidate (active- or idle-mode) UEs available to contribute to the sensing task. The topology thus comprises all nodes whose average channel gain towards the sensing target is at most γdB worse than that of the strongest link, while further ensuring that at least the strongest cell is included to avoid ending up with receivers only. Note that a higher configured value of γgenerally leads to a larger sensing topology, which may enhance the sensing performance. As a drawback, a higher γ may detrimentally impact the communication performance in case it causes more active-mode UEs to aid in sensing, who must thereto forfeit some data reception opportunities. Topology Ω consists of the disjunct sets Ω_{cells} and Ω_{UEs}, comprising the involved cells and UEs, respectively.

While the sensing topology is determined upon initiation of the sensing task and kept fixed throughout its lifetime, the *effective* sensing topology at a given TTI comprises, besides the selected transmit nodes, only those receiver nodes whose receptions are strong enough to enhance the sensing SINR (see below) and hence positively contribute in a fusion towards a bottom-line detection decision. Hence a designated receiver node which receives more interference than sensing signal power and, when included in the fusion process, would worsen the probability of detection, is excluded in the given TTI.

B. Cell selection for communications

In a sense the equivalent of sensing topology management, for the case of communication services cell selection is modelled in a straightforward fashion by associating a given active-mode UE u with cell c_u towards which it has the strongest channel, i.e. $c_u = \underset{c \in \Xi}{\operatorname{argmax}}\, G_{c,u}$.

C. Sensing-communications scheduling

The scheduler coordinates when and which sensing and/or data communication signals are transmitted in the available resources. Assuming wideband scheduling, where each scheduled sensing or communications signal is always assigned the full carrier bandwidth, the considered scheduler covers the time and spatial domain only. It first establishes a periodic transmission schedule for the sensing tasks. For a given sensing task the assigned transmitter nodes concurrently transmit the same sensing signal once every $T_{sensing}$ TTIs. As long as the number $N_{sensing}$ of on-going sensing tasks does not exceed $T_{sensing}$, these periodic transmissions are readily scheduled in a conflict-free manner. If $N_{sensing} > T_{sensing}$ the scheduler will co-schedule (in the same TTI) the transmissions of sensing tasks targeting objects that are farthest apart, to avoid as much as possible overlapping sensing topologies and the need for spatial multiplexing and power sharing. If unavoidable, spatial multiplexing and power sharing will be applied.

Given the determined schedule for periodic sensing signal transmissions, communications transmissions are scheduled for the active-mode UEs. This is done at the cell level, where at each cell proportional fair (PF) scheduling [13] is applied (with exponential smoothing parameter $\alpha = 0.1$) to strike a balance between fairness and resource efficiency. An adaptation [14] of the semi-orthogonal user selection scheme is used [15], which allows the co-scheduling (spatial multiplexing) of one or more communication signals alongside pre-scheduled sensing signals, provided that the corresponding channels satisfy orthogonality threshold $\beta = 0.5$. A key scheduling restriction is imposed by the fact that a UE which is designated as a receiver in a sensing topology must listen for reflections when the corresponding sensing signals are transmitted and hence cannot be scheduled for downlink data transfer in the same TTIs.

D. Beamforming

Each cell applies zero forcing to derive the beamforming precoders for the set of spatially multiplexed (co-scheduled) sensing and communication transmission layers, which in case of a single transmission layer reduces to maximum ratio transmission. A layer is defined as a beamformed transmission by a given transmitter, with multiple signals transmitted by different cells for a given sensing task indeed considered as distinct layers. Layer l transmitted by cell c_l using precoder $\boldsymbol{w}_{c_l,l}(t)$ at TTI t is assigned a per-PRB transmission power of $p_{c_l,l}(t) = p_{\max}/(N_{PRBs} N_{c_l}^{\text{scheduled}}(t))$, given a uniform power split over the $N_{c_l}^{\text{scheduled}}(t)$ spatially multiplexed transmissions.

See Figure 2 for an illustrative example of three cells co-scheduling beamformed sensing (blue) and communication (green) signal transmissions. For the former, the dark-blue signal is the transmitted sensing signal, while the light-blue signals represent the signal reflections off the sensing object.

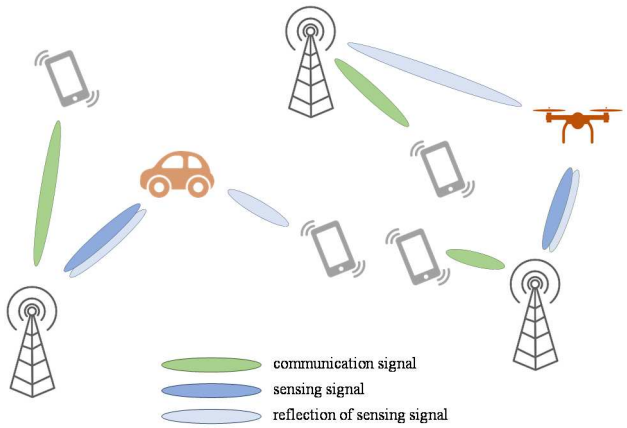

Figure 2: Co-scheduling beamformed sensing and data communication transmission layers.

IV. Performance Assessment

The performance assessment is conducted by dynamically simulating a number of independently generated snapshots. Each such snapshot is characterised by a random placement of a configured number of sensing targets and UEs in the evaluation cells and deriving the associated channel characteristics, including correlated shadowing realisations and randomised small-scale fading traces. Service-specific performance results are aggregated over a sufficiently large number of snapshots to obtain reliable bottom-line results.

A. Sensing performance

The sensing performance is obtained as follows. For each sensing task and for each periodic transmission/reception of the associated sensing signals, the derived SINR is mapped to a probability of detection, as will be outlined below. Scenario-specific average detection probabilities are derived across periodic transmissions, sensing tasks and multiple snapshots.

Consider a sensing task *s* served by a topology comprising a set of transmitters Ω_{cells} and an *effective* set of receivers denoted $\Omega' = \Omega'_{\text{cells}} \cup \Omega'_{\text{UEs}} \subseteq \Omega$, i.e. the union of the set of receiver cells and receiver UEs selected to contribute to sensing fusion, respectively. Assuming that cells are synchronised, the sensing signal reflections received at the different receive antennas of the different receiver cells can be coherently combined. For UEs such synchronisation generally does not hold, hence coherent combining is applied only across the different receive antennas of a given receiver UE, while incoherent combining is applied between a receiver UE and a receiver cell as well as across different receiver UEs. The aggregate power of the sensing signal received at a given TTI *t* and PRB *f* is then given by

$$S(t,f) = \left(\sum_{c\in\Omega_{\text{cells}}} \sum_{c'\in\Omega'_{\text{cells}}} \sum_{r=0}^{R_{c'}-1} \sqrt{S_{c,c',r}(t,f)} \right)^2 + \sum_{c\in\Omega_{\text{cells}}} \sum_{u\in\Omega'_{\text{UEs}}} \left(\sum_{r=0}^{R_u-1} \sqrt{S_{c,u,r}(t,f)} \right)^2,$$

with $S_{c,c',r}(t,f)$ and $S_{c,u,r}(t,f)$ the power level of the sensing signal transmitted by cell *c* as received at antenna *r* of receiver cell *c'* or UE *u*, respectively, and R_m the number of receive antennas at node *m*, i.e. $R_c = 64$ antennas for a cell and $R_u = 4$ antennas for a UE. The former signal power is given by

$$S_{c,c',r}(t,f) = p_{c,s}(t)\left|\boldsymbol{H}_{c,s}(t,f)\boldsymbol{w}_{c,s}(t)\right|^2 \frac{4\pi\sigma}{\lambda^2}\left|\boldsymbol{H}_{s,c',r}(t,f)\right|^2,$$

with $p_{c,s}(t)$ the transmit power of the sensing signal at cell *c*, $\boldsymbol{w}_{c,s}(t)$ the applied precoder and $\boldsymbol{H}_{s,c',r}(t,f)$ the *r*-th element of the channel response vector of the link between the sensing target and receiver cell *c'*. A similar expression holds for $S_{c,u,r}(t,f)$.

The total experienced interference power *I(t,f)* aggregated over all receiver cells and UEs comprises both intra- and inter-cell interference, where the latter can be generated by other evaluation or background cells, and is given by

$$I(t,f) = \sum_{m\in\Omega'} \left(\sum_{\substack{\text{all other}\\ \text{layers } l}} \sum_{r=0}^{R_m-1} p_{c_l,l}(t)\left|\boldsymbol{H}_{c_l,m,r}(t,f)\boldsymbol{w}_{c_l,l}(t)\right|^2 + \sum_{\substack{\text{background}\\ \text{cells } c}} \sum_{r=0}^{R_m-1} p_{BG}\left|\boldsymbol{H}_{c,m,r}(t,f)\boldsymbol{\zeta}_{64}\right|^2 \right),$$

with $\boldsymbol{w}_{c_l,l}(t)$ and $p_{c_l,l}(t)$ the precoder and transmit power applied to (sensing or communications) layer *l*, respectively, and $\boldsymbol{\zeta}_{64}$ the uniform unit vector of length 64, needed to appropriately cope with our simplified antenna modelling for the background cells. In the above expression, 'all other layers' refers to all transmissions not related to the considered sensing task. The expression follows a worst-case assumption that none of the experienced interference is mitigated by smart processing filters.

Assuming incoherent combining across PRBs, the carrier-wide SINR (Signal to Interference plus Noise Ratio) for the considered sensing task at a given TTI *t* is then given by

$$SINR(t) = \frac{\sum_{f=0}^{N_{PRBs}-1} S(t,f)}{\sum_{f=0}^{N_{PRBs}-1}\left(I(t,f) + \left|\Omega'_{\text{cells}}\right|N_{\text{cell}} + \left|\Omega'_{\text{UEs}}\right|N_{\text{UE}}\right)}$$

where N_{cell} and N_{UE} denote the effective noise level per PRB for cell and UE receivers, respectively, including thermal noise (at 290°K) and the node-specific receiver noise figures given above.

Given this *SINR(t)*, the associated probability of detection is derived from Figure 11.4 in [16], using the curve corresponding with the typically assumed false alarm probability of 10^{-6}.

B. Communications performance

Consider now the communications service. As detailed below, at each TTI an SINR is derived for every scheduled UE, which is mapped to a transport block size. At the end of each simulation this yields for each UE an experienced throughput. All these user-level throughputs are gathered over multiple UEs and snapshots to derive the average and 10th percentile values.

For a given data flow to UE *u*, served by cell c_u, the experienced $SINR_u(t,f)$ at TTI *t* and PRB *f* is given by

$$SINR_u(t,f) = \frac{1}{\left(\sum_{r\in R}\left|\boldsymbol{v}_{u,r}(t,f)\right|^2\right)N_{\text{UE}} + I_u(t,f)},$$

where

$$\boldsymbol{v}_u(t,f) = \left(\sqrt{p_{c_u,u}(t)}\boldsymbol{H}_{c_u,u}(t,f)\boldsymbol{w}_{c_u,u}(t)\right)^+$$

denotes UE *u*'s combiner and $\boldsymbol{v}_{u,r}(t,f)$ denotes the combiner's *r*-th element. Interference level $I_u(t,f)$ is given by

$$I_u(t,f) = \sum_{\substack{\text{all other}\\ \text{layers } l}} p_{c_l,l}(t)\left|\boldsymbol{v}_u(t,f)\boldsymbol{H}_{c_l,u}(t,f)\boldsymbol{w}_{c_l,l}(t)\right|^2 + \sum_{\substack{\text{background}\\ \text{cells } c}} p_{BG}\left|\boldsymbol{v}_u(t,f)\boldsymbol{H}_{c,u}(t,f)\boldsymbol{\zeta}_{64}\right|^2.$$

These PRB-specific SINRs are then suitably averaged to obtain carrier-wide $SINR_u(t)$ for UE *u*, utilising the MIESM (Mutual Information Effective SINR Mapping) method [17]. Subsequently, $SINR_u(t)$ is mapped to transport block size $TBS_u(t)$ using an adjusted Shannon formula:

$$TBS_u(t) = \min\left\{TBS_{max}, T_{TTI}\xi B\log_2\left(1 + SINR_u(t)\right)\right\},$$

where TBS_{max} denotes the maximum per-layer transport block size of 57376 bits (cf. Section 5.1.3.2 of [18]) and the correction factor $\xi = 0.75$ is based on [19].

V. Scenarios and Results

A range of scenarios has been simulated to assess the attainable sensing and communications performance and their sensitivity w.r.t. distinct service scenarios and radio resource management configurations. With several parameters already fixed in Section II, all varied parameters are listed in Table I, indicating their value ranges and default setting. Simulation results are given in Figure 3 and will be discussed below.

Consider first the left column of three charts, showing the results for scenarios considering a range of settings for N_{active} and γ, with other parameters set at their default value. The top chart shows the size of the selected (solid curves) and effective (dashed curves) sensing topologies versus sensing topology management parameter γ and for different N_{active}. By design of the algorithm, the sensing topology size increases in γ, noting that for the extreme case of $\gamma = 0$ the topology size exceeds *1* only for the scenarios with $N_{active} > 0$, in which case a UE may provide the strongest link to the sensing target but a cell is still added to the topology to ensure having a transmitter on board. The topology size also increases in N_{active}, due to the higher likelihood of finding a useful UE with a sufficiently strong link to the sensing target. The fraction of receiver nodes excluded in sensing fusion, i.e. the relative size difference between the effective and selected topologies, also increases in N_{active}, due to the higher interference levels and the increased likelihood that a receiver cannot contribute to improve the sensing SINR.

Table I Simulation scenarios.

Parameter	Symbol	Value range
Inter-site distance	*ISD* (m)	{50, …, 125, …, 250}
Propagation environment		{UMi LoS, UMi NLoS}
# active-mode UEs / cell	N_{active}	{0, 1, 2, 3}
# idle-mode UEs / network	N_{idle}	{0, 10, 100, 1000}
# sensing targets / network	$N_{sensing}$	{0, 1, 5, 10}
Radar cross section	σ (m^2)	{1, 10, 100}
Sensing topology management	γ (dB)	{0, 3, 6, 9, 12, 15}

For the same scenarios the centre chart shows the average probability of detection. Observe that the larger topologies selected for a higher γ indeed pay off in terms of an improved probability of detection, up to a threshold of about $\gamma = 9$ dB, beyond which further gains become negligible. For example, for the case with $N_{active} = 0$ the average detection probability increases from about 0.58 for $\gamma = 0$ dB to about 0.74 for $\gamma = 9$-*15* dB. The results further show that the sensing performance worsens for a higher N_{active}. In the given scenario with persistent full-buffer downlink data transfers, an increase in N_{active} causes an increase in the interference level, since with some of the UEs involved in sensing and hence restricted from being scheduled in certain TTIs, having more UEs increases the likelihood that all TTIs are utilised. This interference effect apparently outweighs the gains from an increase in the number of candidate UEs for inclusion in a sensing topology, with an increased potential to select UEs with strong links to the sensing target.

Again considering the same set of scenarios, the bottom chart shows the average and the 10th percentile of the user throughput. Recall that a larger γ implies that more UEs are selected to participate in sensing, are consequently limited in the set of TTIs in which they can be scheduled for downlink data transfer and will therefore experience lower throughputs. As particularly visible for the curve showing the 10th user throughput percentile, this effect is weaker for scenarios with a higher number of active-mode UEs: the higher N_{active}, the smaller the fraction of UEs involved in sensing (see top chart), and hence the lower the throughput impact of the imposed scheduling restrictions. As intuitively obvious, the chart further shows that the throughput performance is worse for higher N_{active}, due to the increased competition for shared resources. Based on these results we select *9* dB as the default setting for sensing topology management parameter γ, as it yields near-optimal sensing performance, without unnecessarily degrading communications performance.

Consider next the top chart in the right column, showing the average probability of detection versus the distance between the sensing target and the strongest cell, now assuming a fixed default setting of $N_{active} = 3$ and $\gamma \in \{0, 3, \ldots, 15\}$ dB. Observe that sensing tasks perform substantially better for targets located nearer to a base station. Observe further that a higher γ and the induced larger sensing topologies indeed improve sensing performance, and increasingly so for targets relatively far from the strongest serving cell, due to the involvement of UEs and, potentially, an additional neighbouring cell.

Consider now the bar chart in Figure 3, which shows a degrading impact of the number of sensing tasks $N_{sensing}$ on the communications performance. The observed degradation is due to a combination of effects: more sensing tasks lead to increased interference levels, reduced resources for data transfer, a higher degree of UE involvement in sensing tasks and consequently fewer data transmission opportunities. Although not shown in a figure, our results further indicate that over the considered range of $N_{sensing}$, the sensing performance remains fairly constant, since for such relatively few sensing tasks, the required sensing signals are either purely time-multiplexed or otherwise spatially multiplexed predominantly across distinct or remote cells, experiencing an insignificant degree of interference.

The bottom-right chart in Figure 3 shows the impact of the ISD and the RCS σ on the sensing performance. When varying the ISD, the antenna tilt is adjusted accordingly to aim towards the cell edge. As is intuitively clear, the performance *(i)* degrades for higher inter-site distances, due to the worsened propagation channel and reduced topology sizes; and *(ii)* improves for higher RCSs, since larger objects reflect more energy and are hence more easily detected. Observe that for a given detection probability target, a substantially sparser network deployment (higher ISD) may suffice if larger objects (higher RCS) are to be detected.

Table II shows the impact of the presence of idle-mode UEs as candidates for involvement in sensing topology selection and

hence contributing to the sensing performance, with all other scenario parameters set to their default values. All shown metrics are averages. These results reveal that a more abundant availability of idle-mode UEs (higher N_{idle}) can substantially enhance the selected/effective topology size and, consequently, the probability of detection. Indirectly, there is also a positive effect on the throughput performance for active-mode UEs, as due to the presence of idle-mode UEs, fewer active-mode UEs are selected to aid in sensing tasks and hence suffer from a reduction in the number of data transmission opportunities.

Table II further includes the results for the case on the UMi NLoS, again assuming otherwise default parameter settings, incl. $N_{idle} = 0$. As intuitively expected, the higher path loss under the NLoS model yields smaller sensing topologies, which along with the worsened path loss itself degrades the sensing performance. The reduction in the sensing topologies further implies that more resources are available for data communications, which, as observed from the enhanced throughput performance, more than compensates for the impact of the increased path loss (which is noted to also reduce not only the desired signal, but also the interference levels).

TABLE II IMPACT OF THE NUMBER OF IDLE-MODE UES (N_{IDLE}) AND THE PROPAGATION ENVIRONMENT.

Metric	*UMi NLoS*	*UMi LoS / N_{idle}*			
		0	**10**	**100**	**1000**
Topology size (# nodes; selected)	2.62	4.91	5.64	14.90	23.04
Topology size (# nodes; effective)	2.01	3.09	3.04	5.26	6.83
Probability of detection	0.37	0.63	0.67	0.75	0.81
User throughput (Mb/s)	10.36	7.26	7.39	7.63	8.52

VI. CONCLUDING REMARKS

We proposed a new configurable topology management algorithm for distributed sensing in a communication-centric ISAC network and presented an extensive scenario-based analysis to quantify the associated performance trade-offs. As shown, the *sensing performance* improves under larger sensing topologies, although gains fade out beyond some point. We further showed the impact of utilising active- and idle-mode UEs in handling sensing tasks, with the presence of the former doing more harm by raising interference levels than contributing to enhanced sensing fusion. In contrast, the exploitation of idle-mode UEs merely has a (potentially substantially) positive effect on the sensing performance. *Communications performance* may degrade substantially in the presence of more sensing tasks and with larger sensing topologies, due to the increased interference levels and the reduction of transmission opportunities to active-mode UEs which aid in sensing tasks. The performance of both sensing and communication services may be improved significantly by reducing inter-site distances and by involving idle-mode UEs as sensing receivers. In future work we will extend of the proposed topology management and resource scheduling solutions to cover e.g. surveillance or tracking tasks.

ACKNOWDLEGMENTS

The authors appreciate the sensing-oriented discussions with Millad Mouri Sardarabadi of the Department of Radar Technologies, TNO, The Netherlands. This research was supported by the National Growth Fund through the Dutch 6G flagship project 'Future Network Services'.

REFERENCES

[1] C. Masouros, J.A. Zhang, F. Liu, L. Zheng, H. Wymeersch and M. Di Renzo (editors), 'Integrated Sensing and Communications for 6G', *IEEE Wireless Communications Magazine*, vol. 30, no. 1, 2023.

[2] A. M. Abouelmaati, S. Aboagye and H. Tabassum, 'Joint spectrum partitioning and power allocation for energy efficient semi-integrated sensing and communications', *IEEE Communications Letters*, vol. 28, no. 7, 2024.

[3] Z. Wei, S. Li, W. Yuan, R. Schober and G. Caire, 'Resource allocation for OTFS-based ISAC systems', *IEEE Transactions on Communications*, vol. 71, no. 3, 2023.

[4] J. Zhang, Z. Fei, X. Wang, P. Liu, J. Huang and Z. Zheng, 'Joint resource allocation and user association for multi-cell integrated sensing and communication systems', *EURASIP Journal on Wireless Communications and Networking*, vol. 2023, no. 1, 2023.

[5] F. Dong, F. Liu, Y. Cui, W.Wang, K. Han and Z.Wang, 'Sensing as a service in 6G perceptive networks: A unified framework for ISAC resource allocation', *IEEE Transactions on Wireless Communications*, vol. 22, no. 5, 2023.

[6] Y. Lyazidi, J. Equi, R. Shreevastav, I. Siomina and G. Fodor, 'ISAC architecture and sensing topology switching in 6G cellular networks', *Proceedings of CSCN '24*, Belgrade, Serbia, 2024.

[7] S. Liu, R. Liu, Z. Lu, M. Li and Q. Liu, 'Cooperative cell-free ISAC networks: joint BS mode selection and beamforming design', *Proceedings of WCNC '24*, Dubai, United Arab Emirates, 2024.

[8] X. Li, Q. Zhu, Y. Chen and Y. Yuan, 'Distributed multi-node cooperative integrated sensing and communication systems: joint beamforming and grouping design', *IEEE Internet of Things Journal*, 2025.

[9] 3GPP, *'Study on channel model for frequencies from 0.5 to 100 GHz'*, TR38.901, v18.0.0, 2024.

[10] F. Gunnarsson, M.N Johansson, A. Furuskär, M. Lundevall, A. Simonsson, C. Tidestav and M. Blomgren, 'Downtilted base station antennas – a simulation model proposal and impact on HSPA and LTE performance', *Proceedings of VTC '08 (Fall)*, Calgary, Canada, 2008.

[11] Fraunhofer, *'Quadriga – The next generation radio channel model'*, www.quadriga-channel-model.de, 2020.

[12] H.-J. Li and Y.-W. Kiang, 'Radar and inverse scattering', in *'The Electrical Engineering Handbook'* (editor: W.-K. Chen), Academic Press, Cambridge, USA,2005.

[13] P. Bender, P. Black, M. Grob, R. Padovani, N. Sindhushyana and A. Viterbi, 'CDMA/HDR: a bandwidth efficient high speed wireless data service for nomadic users', *IEEE Communications Magazine*, vol. 38, no. 7, 2000.

[14] G. Mazzola, *'Radio resource management for joint communication and sensing (JCAS) services in 6G networks'*, MSc thesis, TU Delft, 2024.

[15] T. Yoo and A. Goldsmith, 'On the optimality of multiantenna broadcast scheduling using zero-forcing beamforming', *IEEE Journal on Selected Areas in Communications*, vol. 24, no. 3, 2006.

[16] G. Brooker, *'Introduction to sensors for ranging and imaging'*, SciTech Publishing, Raleigh, USA, 2009.

[17] K. Brueninghaus, D. Astely, T. Salzer, S. Visuri, A. Alexiou, S. Karger and G.-A. Seraji, 'Link performance models for system level simulations of broadband radio access systems', *Proceedings of PIMRC '05*, Berlin, Germany, 2005.

[18] 3GPP, *'Physical layer procedures for data'*, TS38.214, v18.0.0, 2023.

[19] P. Mogensen, W. Na, I.Z. Kovacs, F. Frederiksen, A. Pokhariyal, K.I. Pedersen, T. Kolding, K. Hugl and M. Kuusela, 'LTE capacity compared to the Shannon bound', *Proceedings of VTC '07 (Spring)*, Dublin, Ireland, 2007.

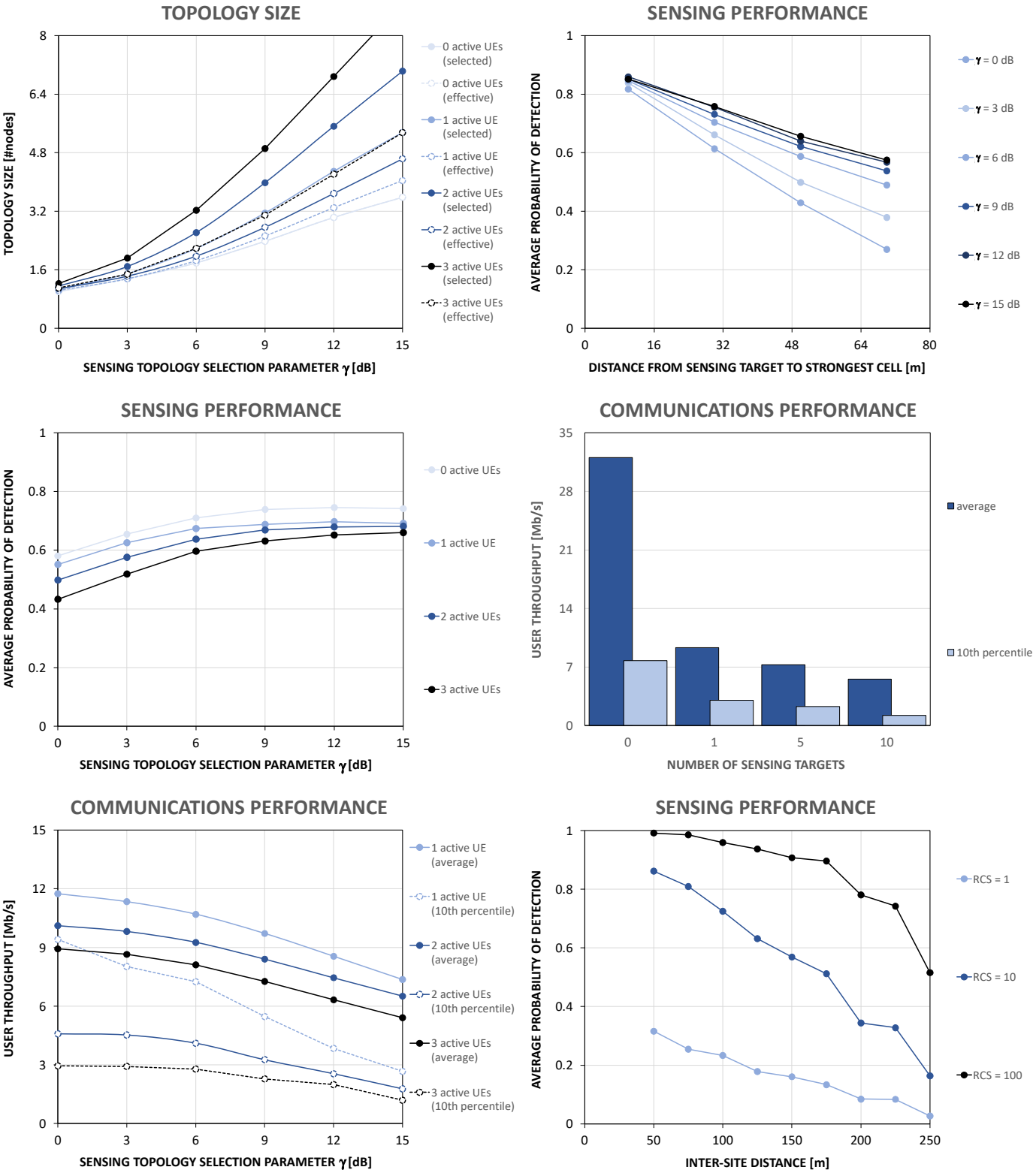

Figure 3: Numerical results.